



RESEARCH ARTICLE

10.1002/2015PA002878

Key Points:

- Deglacial $\Delta^{14}\text{C}$ EEP depth profile had middepth minima during HS1 and YD
- Regional $\Delta^{14}\text{C}$ and $\delta^{18}\text{O}$ gradients require moderately ^{14}C -depleted deglacial EqPIW

Supporting Information:

- Supporting Information S1
- Data Set S1

Correspondence to:

C. M. Lindsay,
Colin.Lindsay@colorado.edu

Citation:

Lindsay, C. M., S. J. Lehman, T. M. Marchitto, J. D. Carriquiry, and J. D. Ortiz (2016), New constraints on deglacial marine radiocarbon anomalies from a depth transect near Baja California, *Paleoceanography*, 31, 1103–1116, doi:10.1002/2015PA002878.

Received 20 OCT 2015

Accepted 20 JUL 2016

Accepted article online 26 JUL 2016

Published online 26 AUG 2016

New constraints on deglacial marine radiocarbon anomalies from a depth transect near Baja California

Colin M. Lindsay^{1,2}, Scott J. Lehman², Thomas M. Marchitto^{1,2}, José D. Carriquiry³, and Joseph D. Ortiz⁴

¹Department of Geological Sciences, University of Colorado Boulder, Boulder, Colorado, USA, ²Institute of Arctic and Alpine Research, University of Colorado Boulder, Boulder, Colorado, USA, ³Instituto de Investigaciones Oceanológicas, Universidad Autónoma de Baja California, Ensenada, Mexico, ⁴Department of Geology, Kent State University, Kent, Ohio, USA

Abstract Previous studies have shown that radiocarbon activities ($\Delta^{14}\text{C}$) in the low-latitude, middepth Pacific and Indian Oceans were anomalously low during Heinrich Stadial 1 (HS1, ~17.8–14.6 ka) and the Younger Dryas (YD, ~12.8–11.5 ka), coincident with intervals of rising atmospheric CO_2 concentration and declining atmospheric $\Delta^{14}\text{C}$. However, a full explanation of these events remains elusive due to sparse and sometimes conflicting data. Here we present new ^{14}C measurements on benthic and planktic foraminifera that, in combination with previously published measurements, enable us to reconstruct the $\Delta^{14}\text{C}$ depth gradient near Baja California. Vertical profiles were similar to present during the Last Glacial Maximum and Bølling/Allerød (14.6–12.8 ka) but display a pronounced middepth (~700 m) $\Delta^{14}\text{C}$ minimum during HS1 and the YD. The latter observation, along with a comparison to other regional reconstructions, appears to rule out intermediate waters from the north or from directly below as proximate sources of aged ^{14}C -depleted ocean carbon during deglaciation and point instead to changes in the composition of Equatorial Pacific intermediate waters. Simple mixing constraints require Equatorial Pacific intermediate waters to be only slightly lower in $\Delta^{14}\text{C}$ than at Baja California, in contrast with previous observations of extremely low $\Delta^{14}\text{C}$ at Galapagos Rise. While the latter may have been influenced by localized releases of geologic (^{14}C -dead) CO_2 , the smaller and more widespread deglacial $\Delta^{14}\text{C}$ anomalies in the Arabian Sea and North Pacific seem to require a source of aged carbon in the glacial deep Southern and Pacific Oceans for which there is growing evidence.

1. Introduction

Radiocarbon (^{14}C) is a rare radioactive isotope of carbon that is naturally produced by cosmic ray interactions in the upper atmosphere, where it is rapidly oxidized to $^{14}\text{CO}_2$ and becomes available for incorporation within the global carbon cycle. The ^{14}C half-life of 5700 years [Godwin, 1962] (National Nuclear Data Center, Brookhaven National Laboratory, www.nndc.bnl.gov) makes it especially useful for quantification of present and past residence times of carbon within global reservoirs that overturn on centennial to millennial timescales, such as the deep ocean. During the last deglaciation, the large fractional increase in atmospheric CO_2 concentration [Monnin *et al.*, 2001; Shakun *et al.*, 2012; Marcott *et al.*, 2014] and the complementary decrease in its ^{14}C activity [Reimer *et al.*, 2013] are both suggestive of a significant redistribution of carbon from an anomalously aged, ^{14}C -depleted, carbon-rich ocean reservoir to the atmosphere [Broecker and Barker, 2007; Marchitto *et al.*, 2007]. Sediment reconstructions indicating periods of very low initial radiocarbon activity (decay-corrected $^{14}\text{C}:^{12}\text{C}$ ratio, expressed as $\Delta^{14}\text{C}$); [Stuiver and Polach, 1977] at intermediate ocean depths near Baja California [Marchitto *et al.*, 2007], the Galapagos Archipelago [Stott *et al.*, 2009], and in the Arabian Sea [Bryan *et al.*, 2010] have been interpreted as evidence of this redistribution process, with aged, excess carbon upwelled from a presumed abyssal reservoir in the Southern Ocean and transported (at least in part) to low latitudes via Antarctic Intermediate Water (AAIW).

Observational support for a ^{14}C -depleted reservoir of excess carbon in the deep glacial Southern and Pacific Oceans continues to mount [Sikes *et al.*, 2000; Skinner *et al.*, 2010, 2014; Burke and Robinson, 2012; de la Fuente *et al.*, 2015; Keigwin and Lehman, 2015; Ronge *et al.*, 2016], and there is also strong evidence for transiently high CO_2 and nutrient concentrations in intermediate waters originating from the Southern Ocean during deglaciation [Spero and Lea, 2002; Anderson *et al.*, 2009; Allen *et al.*, 2015; Carriquiry *et al.*, 2015; Martínez-Botí *et al.*, 2015]. However, complementary evidence for anomalously low $\Delta^{14}\text{C}$ near AAIW source areas in the Southern Hemisphere is still lacking [De Pol-Holz *et al.*, 2010; Rose *et al.*, 2010; Cléroux *et al.*, 2011; Sortor

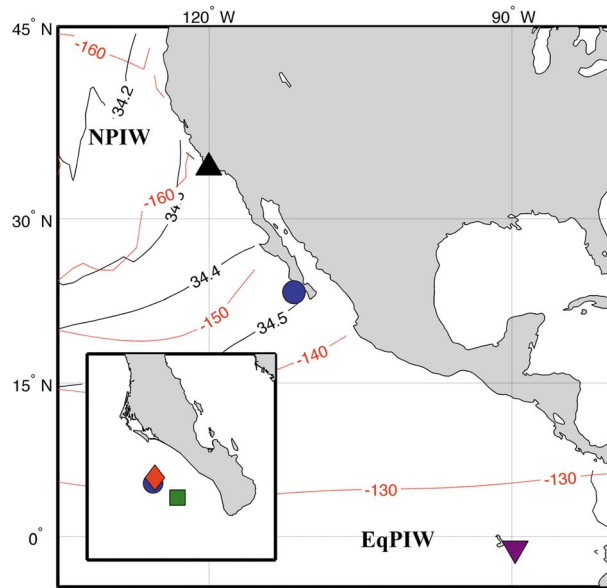


Figure 1. Symbols show the locations of sediment cores with benthic records discussed in this paper, plotted with contoured mean salinity (practical salinity unit, solid black lines, World Ocean Atlas 2013 (WOA13) [Zweng *et al.*, 2013] and estimated natural radiocarbon (per mil, red dashed lines, GLODAP) [Key, 2004] of waters with density anomaly (σ_θ) values of $27.1 \pm 0.05 \text{ kg/m}^3$. Inset shows a zoomed-in view of core locations near Baja California. Cores shown are Santa Barbara Basin core ODP893A (black triangle) [Hendy and Kennett, 2003], Baja California cores MV99-MC19/GC31/PC08 (blue circle), MV99-PC10 (red diamond) and MV99-GC38 (green square) [Van Geen *et al.*, 2003], and Galapagos Rise core VM21-30 (purple inverted triangle) [Koutavas *et al.*, 2006]. Regions are labeled where North Pacific Intermediate Water (NPIW) and Equatorial Pacific Intermediate Water (EqPIW) occupy this density layer.

contributions from local geologic sources. Taken together, our analysis suggests that transient deglacial $\Delta^{14}\text{C}$ minima off Baja California were not caused by upward mixing of North Pacific Deep Water or lateral addition of North Pacific Intermediate Water and were more likely influenced by waters coming from the Equatorial Pacific, with a probable origin in the deep Southern and Pacific Oceans.

1.1. Study Site and Regional Context

Cores MV99-PC10, MV99-PC08, and MV99-GC38 form a depth transect at modern water depths of 432, 705, and 1270 m, respectively, on the western margin of Southern Baja California (van Geen *et al.*, 2003). The core sites lie near the present-day mixing boundary of fresh, cold North Pacific Intermediate Water (NPIW) and salty, warm Equatorial Pacific Intermediate Water (EqPIW). In an effort to characterize these two water masses (or their regional analogs) in the past, we also discuss published data from two sediment cores retrieved from intermediate water depths to the north and south of Baja California: Santa Barbara Basin core ODP893A (SBB, 34°N, modern sill depth 475 m) [Hendy and Kennett, 2003] and Galapagos Rise core VM21-30 (1°S, 617 m) [Koutavas *et al.*, 2006; Stott *et al.*, 2009].

Figure 1 shows the locations of these cores with respect to contoured salinity values and estimated “natural” (i.e., preindustrial and pre-nuclear) $\Delta^{14}\text{C}$ of waters in the 27.1 kg/m^3 σ_θ density anomaly layer which occupies a mean depth of ~625 m along the eastern Pacific margin, close to that of the relevant core (and sill) depths. At this density level the deepest and densest NPIW circulates clockwise from its formation region in the northwest northern Pacific [Talley, 1993; You, 2003; Bostock *et al.*, 2010]. The saltier EqPIW south of Baja California is formed by mixing between Antarctic Intermediate Water (AAIW) and North Pacific Deep Water (NPDW) [Bostock *et al.*, 2010] in narrow intermediate-depth zonal jets passing through the shadow zone within ~10° of the equator [Firing *et al.*, 1998; Cravatte *et al.*, 2012]. Both NPIW and EqPIW overlie NPDW with a transitional boundary between ~1000 and 1500 m [Fiedler and Talley, 2006; Bostock *et al.*,

and Lund, 2011; Burke and Robinson, 2012; Siani *et al.*, 2013]. Adding to the problem is the growing suspicion that the ^{14}C signal from at least one intermediate-depth location off of the Galapagos Archipelago has been influenced by local sources of volcanic CO_2 , leading to anomalously low $\Delta^{14}\text{C}$ values [Stott and Timmermann, 2011]. Consequently, our understanding of previously observed deglacial radiocarbon anomalies remains incomplete.

Here we present time series of ^{14}C measurements and estimated initial $\Delta^{14}\text{C}$ from cores near Baja California that, together with previous results from Marchitto *et al.* [2007] and Lindsay *et al.* [2015], constitute a depth transect from the surface to 1270 m modern water depth, enabling us to constrain the local vertical gradients of $\Delta^{14}\text{C}$ during deglaciation. We also present a high-resolution benthic oxygen isotope record that, in the context of $\delta^{18}\text{O}$ and $\Delta^{14}\text{C}$ records from other sediment cores, provides information on the lateral mixture of water masses near Baja California and likely regional end-member $\Delta^{14}\text{C}$ values, none of which would seem to require anomalous con-

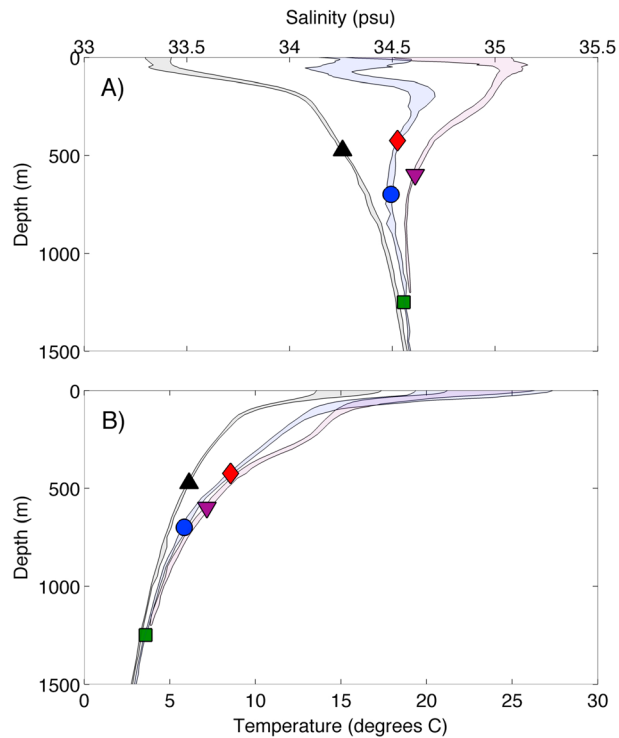


Figure 2. Shaded envelopes show the annual range of monthly (a) mean salinity and (b) temperature depth profiles from WOA13 grid cells closest to the three core locations shown in Figure 1. The water or sill depths of all marine cores discussed in this paper are indicated by filled symbols on the matching profiles. Symbols and colors are the same as in Figure 1.

2010]. Nearer the surface, the California Undercurrent (CU) carries warm, high-salinity Equatorial Subsurface Water (ESSW) north along the shelf break near Baja California [Hickey, 1979; Lynn and Simpson, 1987], raising subsurface temperatures and salinities in waters with densities ranging from ~ 25.5 to $27.2\sigma_\theta$ and at depths of ~ 100 – 500 m (Figures 2 and 3). The ESSW in the CU is probably sourced from the northern Tsuchiya jet (also known as the Northern Subsurface Countercurrent), an eastward flowing jet just below the Equatorial Pacific thermocline that carries a mixture of AAIW, high-salinity North Pacific Eastern Subtropical Mode Water, and, possibly, also NPIW [Fiedler and Talley, 2006].

Mixing between northern and equatorial waters is clearly evident in climatological salinity and temperature profiles along the Eastern Pacific margin [Locarnini et al., 2013; Zweng et al., 2013] (Figures 2 and 3), connecting Baja California to the Galapagos at intermediate and shallow depths through the saltier water masses (EqPIW and ESSW) and to the Santa Barbara Basin through the fresher water masses (CC

and NPIW). At the location and depth of our Baja California transect, absolute S and T values suggest a greater contribution of EqPIW than NPIW, while ESSW carried by the CU dominates in shallower depths up to ~ 100 m. NPIW in its strict sense (defined by a salinity minimum at intermediate depth) is not observed this far east in the modern North Pacific [Talley, 1993; You, 2003], but we will follow other authors [e.g., Hendy and Kennett, 2003; Bostock et al., 2010] and use the term NPIW for the fresher North Pacific water affecting the California margin at intermediate depths.

2. Methods

2.1. ^{14}C and Derived Values

Monospecific samples of the planktic foraminifer *Globigerinoides ruber*, as well as samples of the benthic foraminifera *Uvigerina* spp., were picked from the $>250\ \mu\text{m}$ size fraction of washed sediment from cores MV99-PC10 and MV99-GC38. In some cases, samples that were too small for radiocarbon measurement were brought up to weight by adding foraminifera from the 150 – $250\ \mu\text{m}$ size fraction. All ^{14}C samples were prepared at the Institute of Arctic and Alpine Research Laboratory for Accelerator Mass Spectrometry (AMS) Radiocarbon Preparation and Research before measurement at the Keck Carbon Cycle AMS (KCCAMS) Laboratory at the University of California, Irvine. Picked foraminifera were leached for 5 min in a $0.001\ \text{M}$ solution of HCl. Each sample was then reacted with H_3PO_4 , and the CO_2 produced was cryogenically purified. The purified CO_2 was reduced with H_2 in the presence of a Fe catalyst, and the resulting graphite mixture was packed into AMS targets and sent to KCCAMS.

Benthic-Planktic (B-P) age differences were calculated by subtracting the conventional planktic ^{14}C age from the conventional benthic ^{14}C age in samples where both were measured. In cases where benthic and planktic measurements were not paired directly, B-P age differences were estimated by subtracting the linearly

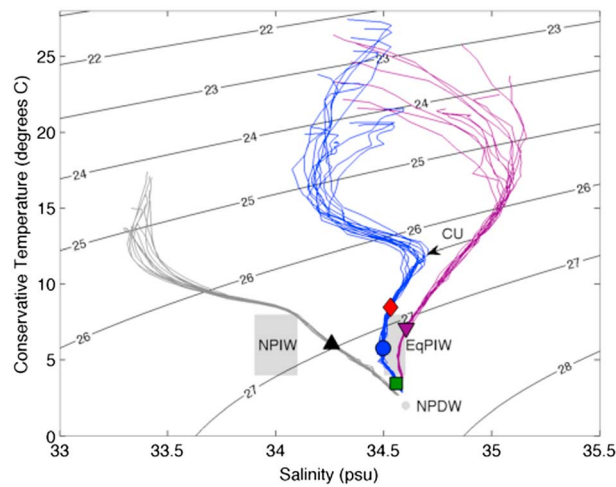


Figure 3. WOA13 monthly mean temperature profiles plotted versus monthly mean salinity for the three core locations, with contoured density anomaly (σ_θ) values. Cores are plotted at their annual mean values according to the WOA13 grid cell closest to their location and water or sill depth, with the same symbols as in Figure 1. Gray labeled rectangles and small filled circles show salinity and temperature ranges of NPIW, EqPIW, and a point estimate of NPDW temperature and salinity, all from *Bostock et al.* [2010]. The transport of ESSW by the California Undercurrent (CU) is represented by a labeled arrow. Density anomaly was estimated using the Gibbs Seawater Oceanographic Toolbox [MacDougall and Barker, 2011].

dried, and stored in vials. Before analysis, foraminifera samples were heated to 350°C for 2 h, at atmospheric pressure, in order to remove hydrolyzable organic matter. Samples were then reacted to generate carbon dioxide in a common bath of orthophosphoric acid at 90°C (specific gravity = 1.92 g cm⁻³). During each run sequence, an in-house standard MIO Marble calibrated against NBS-19 (National Bureau of Standards) was used to correct the data, including a drift correction. Corrected delta values are expressed in per mil relative to PDB (Pee Dee belemnite) international standards for $\delta^{13}\text{C}$ and $\delta^{18}\text{O}$. The external precision of the isotopic measurements was <0.04‰ for both $\delta^{18}\text{O}$ and $\delta^{13}\text{C}$. A low-resolution version of this record has previously been published in a compilation of stable isotope measurements from near Baja California [Carriquiry et al., 2015].

2.3. Diffuse Spectral Reflectance

Diffuse spectral reflectance (DSR) for all MV99 Baja California cores was measured shipboard using a Minolta CM-2022 spectrophotometer with 1 cm resolution [Ortiz et al., 2004]. Measurements were conducted on the wet, split surfaces of the sediment cores, which were wrapped in GladWrap™ to prevent contamination of the instruments integration sphere. The DSR measurements were decomposed using a three-component R-mode factor model of the first-derivative transform of the percent reflectance spectra, which is analogous to a varimax-rotated, principle component analysis. The methodology employed with DSR data is more fully described in Ortiz [2011]. Empirical correlation documents that DSR Factor 3 is closely related to down core variation of organic carbon concentration and bears a strong resemblance to Greenland oxygen isotope records [Ortiz et al., 2004], a finding that was previously used to tie core PC08 to the GISP2 layer-counted calendar age model [Marchitto et al., 2007].

2.4. Age-Depth Modeling

Calendar age models for the Baja California cores PC10 and GC38 were constructed by tying them to the GISP2-based age model for PC08 [Marchitto et al., 2007]. This was achieved primarily by mapping of planktic ¹⁴C results from cores PC10 and GC38 onto those for PC08 [Lindsay et al., 2015], based on the expectation that local gradients in $\Delta^{14}\text{C}$ of near-surface waters between the three core locations remained negligible and that local surface reservoir ages were well characterized by Lindsay et al. [2015]. We supplemented the age

interpolated planktic ¹⁴C age from the benthic ¹⁴C age measured at a given level. Decay-corrected initial radiocarbon activities ($\Delta^{14}\text{C}$) [Stuiver and Polach, 1977] were calculated for all deglacial ¹⁴C results, using the measured conventional ¹⁴C age and estimates of calendar age and its uncertainty from age-depth modeling described below (section 2.4).

2.2. Stable Isotopes

Stable isotope ratios of carbon and oxygen were measured in monospecific samples of *Uvigerina peregrina* from core PC08 on an OPTIMA mass spectrometer interfaced to an automated common acid bath (ISOCARB) at the Instituto de Investigaciones Oceanológicas of the Universidad Autónoma de Baja California, Mexico. Between 5 and 11 foraminifera tests within the 125–250 μm size fraction were used for each isotopic analysis. Picked foraminifera were ultrasonically cleaned in distilled water to free adhering particles, oven

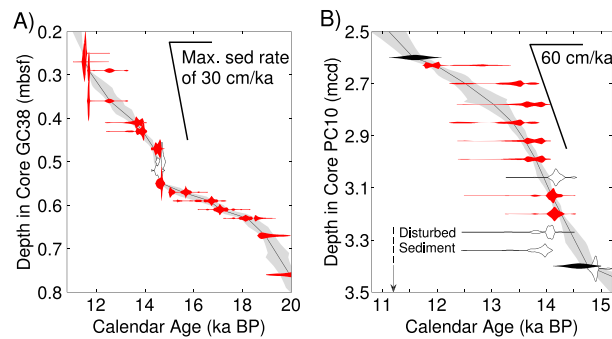


Figure 4. Age models for (a) core GC38 and (b) core PC10. Filled shapes show the probability density distributions of calendar age versus depth in core from DSR tie points (filled black) and *G. ruber* ¹⁴C (filled red) that were used to construct each age model. Distributions from *G. ruber* ¹⁴C dates that were left out of the Monte Carlo age model step are plotted as empty white shapes. The age models resulting from Monte Carlo filtering and interpolation (see text for details) are shown by the solid black lines and gray 1 sigma uncertainty envelopes.

Globigerinoides sacculifer revealed large changes in apparent reservoir age during deglaciation, with *G. ruber* generally showing the most coherent (least noisy) trends over time [Lindsay et al., 2015]. We thus use the PC08 *G. ruber* ¹⁴C-calendar age relationship as a species-specific local reference curve in order to derive calendar age estimates for the other cores, free of assumptions regarding the magnitude and uncertainty of past reservoir ages that are otherwise required of conventional marine ¹⁴C calibration algorithms. To create the local reference curve, the PC08 *G. ruber* record was interpolated between ¹⁴C measurements using a Monte Carlo approach that allowed for greater uncertainty at points farther from measurements (see supporting information). *G. ruber* ¹⁴C measurements from PC10 and GC38 were then mapped onto the reference curve using the standard statistical method recommended for use with INTCAL calibration curves [Stuiver et al., 2005], resulting in probability density distributions (PDFs) of calendar age for each measurement.

The PCA Factor 3 of the diffuse spectral reflectance (DSR) of Baja California cores is closely tied to organic carbon content, and its down core variation most likely indicates changes in regional productivity during deglaciation [Ortiz et al., 2004]. It is therefore reasonable to expect that changes in DSR Factor 3 should have occurred in all three cores more or less simultaneously, although the signal may be expected to decrease with depth below the oxygen minimum zone. We chose DSR tie points between the two new cores and PC08, with estimated normally distributed 1σ age uncertainties of ±200 years. In core GC38, no DSR-based tie points younger than ~32 ka were assigned (see supporting information Figure S2), permitting the use of DSR agreement during deglaciation as an independent check on the planktic ¹⁴C-based match to the PC08 age model. In core PC10, two DSR tie points were used in the deglacial interval because of insufficient planktic abundance in the uppermost section and ¹⁴C age reversals in the lower section.

¹⁴C- and DSR-derived PDFs are shown against depth for the deglacial sections of the target cores in Figure 4. ¹⁴C-derived PDFs are broad in many cases due to the presence of age plateaus in the planktic ¹⁴C record from PC08 (supporting information Figures S1 and S2). A population of age-depth models was created by randomly selecting ages from the individual PDFs using a Monte Carlo approach but discarding any age model resulting in an age reversal or intervals of excessively high sedimentation rate. For the upper bounds of the sedimentation rate filter, we used 30 cm/ka for GC38 and 60 cm/ka for PC10. To account for the fact that age uncertainties will be larger with core distance from levels with either ¹⁴C- or DSR-derived PDFs, we interpolated between these levels in both directions using a second Monte Carlo step that randomly sampled a population of sedimentation rates defined by the mean and 1σ standard deviation of all previously permitted realizations of the sedimentation rate in a particular core. In essence this assumes that the low-frequency variability in sedimentation rate revealed by our age-depth modeling is a reasonable approximation of the potential high-frequency variability between depths with explicit age control. The resultant set of age models are depicted by the black line with gray envelope (median age and 1σ range) for each core in Figure 4.

controls with tie points from between-core correlation of sedimentary reflectance data only where ¹⁴C results were unavailable due to low carrier abundance or showed significant scatter (see supporting information Figures S1 and S2). Reflectance data were otherwise reserved for post facto evaluation of the ¹⁴C-derived age models. We used the planktic ¹⁴C as the primary age control because DSR provides strong age constraints only during times of rapid change, usually at climate interval boundaries, and thus provides lower resolution age control.

In previous work, PC08 ¹⁴C results for the planktic foraminifera *Globigerinoides ruber*, *Globigerina bulloides*, and

In GC38, the raw ^{14}C data are relatively smooth throughout the deglacial period (see supporting information Figure S1), suggesting that sedimentation was continuous over that interval, although the probability density distributions of age for *G. ruber* ^{14}C in GC38 indicate a period of rapid sedimentation around 14.5 ka. We omitted the middle two *G. ruber* ^{14}C dates in this segment from our calculations to reduce the computation time needed to accumulate a large number of realizations passing the sedimentation rate filter (see Figure 4). Because of the relatively high sedimentation rate implied by the bracketing measurements, the ages of the intervening depths are still well constrained.

In PC10, the section below about 4.5 mcd was previously found to contain a hiatus [Van Geen *et al.*, 2003], possibly because of winnowing at the core location during the period of low sea level prior to ~15 ka [Dean *et al.*, 2006]. Our ^{14}C measurements between 4.5 and 3.4 mcd are scattered and contain multiple age reversals (supporting information Figure S2) and a very large negative B-P age (–1300 ^{14}C years at 3.41 mcd). We considered this evidence that sedimentation was disturbed up to at least 3.4 mcd and excluded deeper results from all following figures. One ^{14}C -derived PDF at 3.06 mcd and two from below 3.2 mcd were omitted from the Monte Carlo calculations to reduce computation time (Figure 4). The two *G. ruber* PDFs below 3.2 mcd cause an age reversal that hints that the sediment disturbance may extend up to about 3.2 mcd but is not conclusive. Therefore, we indicate potential sediment disturbance below 3.2 mcd in Figure 4 and supporting information Figure S2 but retain the data from between 3.2 and 3.4 mcd in our results figures. The revised age model for PC10 places the start of undisturbed sedimentation in PC10 at ~14.3–14.6 ka (Figure 4).

It is important to note that the primary aim of the age-depth modeling here is to create a common chronology that attempts to minimize between-core differences of estimated calendar age during the deglacial study interval rather than to derive the most accurate possible estimate of absolute calendar age and age uncertainty. Thus, we do not attempt to propagate additional uncertainty or bias associated with the underlying PC08 and GISP2 age models. Any such shared biases would have only a very small influence on reconstructed vertical $\Delta^{14}\text{C}$ gradients between cores, since individual $\Delta^{14}\text{C}$ estimates assigned to similar calendar ages in different cores would move along age-decay trajectories together.

3. Results and Discussion

3.1. Internal Consistency

Planktic and benthic $\Delta^{14}\text{C}$ values and sedimentation rates depend explicitly on our age modeling. DSR and B-P age difference values do not, although the age models will dictate their patterns through time. We therefore assess the success of the alignment on the common age model by comparing results between the three Baja California cores, as well as between planktic $\Delta^{14}\text{C}$ and INTCAL13 atmospheric $\Delta^{14}\text{C}$ [Reimer *et al.*, 2013] (Figure 5). Similar estimates of *G. ruber* $\Delta^{14}\text{C}$ for cores PC08 and GC38 confirm that the local ^{14}C age-based method of mapping the calendar age model from core PC08 into GC38 will deliver comparable $\Delta^{14}\text{C}$, as expected based on our a priori assumptions. The same is true of core PC10 but with somewhat larger discrepancies as a result of disturbed sediment older than about 14.3 ka B.P. and use of a DSR tie point at 11.6 ka B.P.

When placed on the common age model, the timing of changes in B-P ^{14}C age difference (Figure 5e) is also similar between the three cores, suggesting that there are not large intercore biases in the chronologies. In addition, changes in DSR Factor 3 during the deglacial study interval in GC38, which as noted earlier were not used for derivation of the age model after ~30 ka, are consistent with DSR changes seen in PC08 (Figure 5c). The same is true for DSR variations in PC10 between assigned DSR tie points at ~11.6 and 14.6 ka, providing additional confidence in the age alignment of all three cores.

3.2. Sedimentation Rate Variations

Variations of sedimentation rate in PC10 and GC38 (Figure 5d), while large, are consistent with the DSR changes measured in PC10 and GC38 (Figure 5c), which indicate higher productivity during the Bølling Allerød (BA) and lower productivity during Younger Dryas (YD) and Heinrich Stadial 1 (HS1) [Ortiz *et al.*, 2004] (see also supporting information Text S2 and Figure S3). The relatively constant sedimentation rate history of PC08 is due to the fact that dry bulk density is observed to decrease in association with increasing organic carbon content, which would act to reduce apparent variations of sedimentation rate associated with primary production [Ortiz *et al.*, 2004]. The original PC08 age model nonetheless indicates a sedimentation

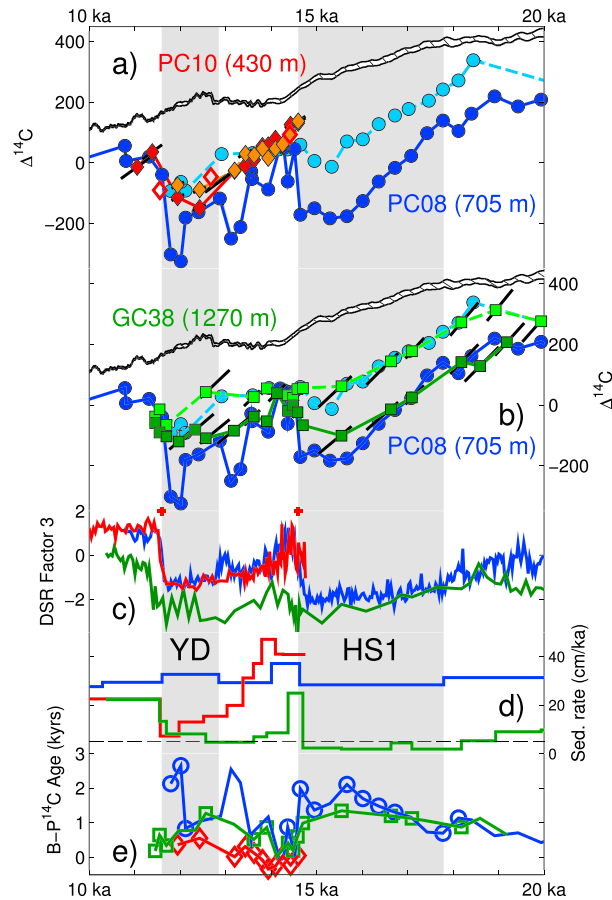


Figure 5. Results from the Baja California margin plotted versus time. (a) *Uvigerina* spp. (red filled diamonds), mixed benthic (open red diamonds), and *G. ruber* (orange filled diamonds) $\Delta^{14}\text{C}$ from core PC10 (432 m) compared to benthic (dark blue filled circles) and *G. ruber* (light blue filled circles) $\Delta^{14}\text{C}$ from core PC08 (705 m) [Lindsay et al., 2015; Marchitto et al., 2007] and INTCAL13 atmospheric $\Delta^{14}\text{C}$ (hatched field) [Reimer et al., 2013]. Solid black error lines for PC10 data represent the effect of uncertainty relative to the PC08 age scale and are calculated using the 1 sigma endpoint values for ^{14}C measurement and calendar age. In some instances the error bars are small and hidden by the symbols. (b) Benthic (dark green filled squares) and *G. ruber* (light green filled squares) $\Delta^{14}\text{C}$ from core GC38 (1270 m) compared to *G. ruber* (light blue filled circles) and benthic (dark blue filled circles) $\Delta^{14}\text{C}$ from core PC08 and INTCAL13 atmospheric $\Delta^{14}\text{C}$ (hatched field). Solid black error lines for GC38 data represent the effect of uncertainty relative to the PC08 age scale and are calculated using the 1 sigma endpoint values for ^{14}C measurement and calendar age. In some instances the error bars are small and hidden by the symbols. (c) PC10 (red line), GC38 (green line), and PC08 (blue line) DSR Factor 3. To aid visual comparison over this time period, GC38 DSR Factor 3 was shifted toward the other records by adding 4 normalized units. (d) PC10 (red line), GC38 (green line), and PC08 (blue line) accumulation rates. The thin dashed black line indicates the 5 cm/ka level. Red plus signs mark the ages of two DSR-based tie points used in the PC10 age model. (e) PC10 paired B-P ages (red open diamonds and red line), all (green line) and paired only (open green squares) GC38 B-P ages (green open squares), and all (blue line) and paired only (open blue circles) PC08 B-P ages. B-P uncertainty is much smaller than the symbols. Gray vertical fields indicate the age ranges of Heinrich Stadial 1 (HS1) and the Younger Dryas (YD).

rate during the early BA that is $\sim 30\%$ higher than the average rate for the core. The general pattern of sedimentation rate changes suggested by our age models is also consistent with mass accumulation rates of biogenic material in cores from much of the North Pacific, which indicate a large productivity spike during the BA [Kohfeld and Chase, 2011].

3.3. B-P Age Differences

Raw ^{14}C age differences between benthic foraminifera and those of codeposited planktic foraminifera (or for interpolated planktic ages) show broadly similar time-dependent patterns for all cores but are frequently largest in core PC08 from 705 mwd (Figure 5e). Given the use of a single planktic species for planktic ^{14}C measurements and our a priori assumption that lateral gradients of surface water $\Delta^{14}\text{C}$ within the Baja California region were negligible, differences of B-P age between cores PC10, PC08, and GC38 are expected to reflect primarily differences of benthic foraminifera age and thus gradients in ^{14}C age of bottom waters bathing the different sites.

The slightly negative and near-zero B-P ages that we observe in PC10 during the early BA (-300 to 50 ^{14}C years) may well be reliable, reflecting a combination of lower sea level and larger seasonal variation in near-surface $\Delta^{14}\text{C}$ during the BA than at present. For example, Lindsay et al. [2015] observed planktic interspecies $\Delta^{14}\text{C}$ differences of $60\text{--}100\text{‰}$ ($\sim 400\text{--}700$ ^{14}C years) during deglaciation that they attributed to large $\Delta^{14}\text{C}$ differences between the northern and southern source waters that seasonally affected the upper water column near core PC08. Lowest values were recorded by *G. ruber*, reflecting the larger reservoir age (lower $\Delta^{14}\text{C}$) of upwelling southern-sourced waters during late summer and fall when this species is thought to be most abundant [Lindsay et al., 2015]. Global eustatic sea levels that were then ~ 90 m lower than today [Fleming et al., 1998] may also

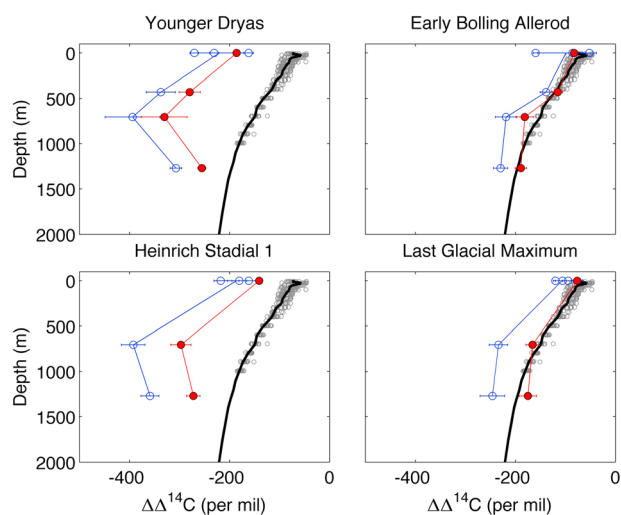


Figure 6. Average $\Delta\Delta^{14}\text{C}$ depth profiles from Baja California cores compared to modern observations. Depth profiles of reconstructed $\Delta\Delta^{14}\text{C}$ (blue lines and open circles, calculated as core $\Delta^{14}\text{C}$ minus coeval INTCAL13 atmospheric $\Delta^{14}\text{C}$) and atmospheric $\Delta^{14}\text{C}$ normalized $\Delta\Delta^{14}\text{C}$ (red lines and filled circles) are shown averaged over four time periods (YD: 12.85–11.6 ka, early BA: 14.6–13.5 ka, HS1: 17.8–14.6 ka, and LGM: 20–17.8 ka). For clarity only unnormalized $\Delta\Delta^{14}\text{C}$ averages are plotted at the surface for all three planktic species measured in PC08; the central surface value that each depth profile connects to is the average of the three planktic values from that time period. Horizontal error bars are the standard error of the mean. Because of disturbed sediment (see section 2.4), no results are plotted from PC10 (430 m) during HS1 and the LGM. Estimated preindustrial, pre-nuclear $\Delta\Delta^{14}\text{C}$ GLODAP bottle data [Key, 2004] from sites just south of Baja California (24–17°N) are plotted in each panel along with a depth profile from GLODAP gridded preindustrial, pre-nuclear $\Delta\Delta^{14}\text{C}$ data (heavy black line) [Key, 2004] from the grid cell 1° west of the site of GC38 (necessary because of the resolution of GLODAP bathymetry.) No adjustment was made to the profiles to account for changing water depths due to lower sea levels in the past.

3.5. Vertical $\Delta^{14}\text{C}$ Gradients

To visualize the $\Delta^{14}\text{C}$ depth gradient over time, we averaged the difference between estimated benthic foraminiferal $\Delta^{14}\text{C}$ for the available Baja California records and that of the coeval atmosphere [Reimer et al., 2013] over the time periods YD, early BA (14.6–13.5 ka), HS1, and the Last Glacial Maximum (LGM, here defined as 20–17.8 ka with an upper age limit based on the length of the GC38 benthic record). Time-averaged offsets from the atmosphere are expressed as $\Delta\Delta^{14}\text{C}$ and compared to the closest depth profiles of estimated natural $\Delta^{14}\text{C}$ from the Global Data Analysis Project (GLODAP) [Key, 2004] in Figure 6.

Some degree of negative deviation of $\Delta\Delta^{14}\text{C}$ from the modern profile (including the surface) may be expected as a result of both reduced atmospheric CO_2 concentration and elevated atmospheric ^{14}C activity relative to today. Given constant gas transfer velocity, the air-sea exchange of CO_2 (and the associated isotopic exchanges) will scale directly to the atmospheric CO_2 burden. Thus, lower CO_2 levels during the LGM and deglaciation should be expected to produce slightly lower $\Delta\Delta^{14}\text{C}$ at the ocean surface (i.e., greater surface reservoir age) [Bard, 1988; Galbraith et al., 2015] and also at depth where isotopic signatures were influenced by surface conditions in outcrop regions elsewhere. Elevated atmospheric $\Delta^{14}\text{C}$ may also be expected to decrease $\Delta\Delta^{14}\text{C}$ at depth for any given absolute ventilation age (time since surface equilibration) due to the exponential dependence of radioactive decay on initial ^{14}C activity. We corrected our reconstructions for the latter effect following the method detailed in Burke et al. [2015], resulting in profiles of atmospheric $\Delta^{14}\text{C}$ normalized $\Delta\Delta^{14}\text{C}$ (red profiles in Figure 6). The close agreement between the modern profile and

have caused benthic foraminifera in the shallow PC10 core location to experience seasonal $\Delta^{14}\text{C}$ changes comparable to those at the surface. However, in contrast to the planktic species, the benthic species are expected to calcify throughout the year. Thus, negative B-P ages during the early BA may reflect the difference between the negative extreme (*G. ruber*) and mean value (benthics) of the seasonal cycle of $\Delta^{14}\text{C}$ near the surface.

3.4. $\Delta^{14}\text{C}$ Results

As suggested by the B-P ages, the $\Delta^{14}\text{C}$ results from core GC38 reveal that $\Delta^{14}\text{C}$ at 1270 m water depth was low relative to the atmosphere but 100–200‰ higher than that in PC08 during the anomalous depletion events of HS1, the late BA, and the YD (Figure 5b). Benthic $\Delta^{14}\text{C}$ in PC10 was likewise ~150‰ lower with respect to atmosphere during the YD than during the BA but was consistently 50–200‰ higher than that in PC08 during the late BA and YD (Figure 5a). This suggests that the most ^{14}C -depleted waters near Baja California during transient $\Delta^{14}\text{C}$ anomalies occurred in the vicinity of core PC08 (705 m), with a $\Delta^{14}\text{C}$ minimum somewhere between the depths of cores GC38 (1270 m) and PC10 (420 m).

normalized $\Delta\Delta^{14}\text{C}$ during the LGM and the BA suggests that much of the difference between the modern and unnormalized $\Delta\Delta^{14}\text{C}$ profiles for these intervals can be explained by higher initial activity and that significant changes in the regional circulation of the upper ocean are not required.

The average gradients during HS1 and the YD had a notably different structure, with substantially lower $\Delta\Delta^{14}\text{C}$ at every depth and a conspicuous minimum at middepth (shallower than 1270 m modern water depth). During the YD, the addition of data from PC10 also allows us to constrain the $\Delta^{14}\text{C}$ minimum to deeper than 430 m modern water depth. The large negative deviation from the modern profile and the middepth $\Delta\Delta^{14}\text{C}$ minimum are together indicative of significant changes in source water $\Delta^{14}\text{C}$ and, possibly, in the physical circulation.

Waters at depths of 500–1000 m near Baja California today are influenced predominately by EqPIW and NPIW, while unmodified NPDW lies beneath a transition zone at ~1000–1500 m (see section 1.1). As can be seen from the modern $\Delta^{14}\text{C}$ gradient (Figure 6), modern NPDW (water deeper than ~1500 m) has lower $\Delta^{14}\text{C}$ than modern intermediate water near Baja California. The profiles observed during HS1 and the YD suggest a reversed vertical $\Delta^{14}\text{C}$ gradient between waters near 1270 mwd and the overlying intermediate waters. A previous study also found evidence of a reversed $\Delta^{14}\text{C}$ gradient between 1600 and 800 m near central California during late deglaciation, possibly corresponding to the YD anomaly we observe and suggesting a broad regional pattern [van Geen *et al.*, 1996].

It is possible that relatively high- $\Delta^{14}\text{C}$ water at 1270 mwd off of Baja may have originated in the North Pacific as a result of middepth convection during HS1 and the YD [Okazaki *et al.*, 2010; Rae *et al.*, 2014] and may have lain above more depleted deglacial NPDW. Specifically, regional deep water at 2.9 km in the North Pacific [de la Fuente *et al.*, 2015] may have been more depleted than at 1270 mwd off of Baja, suggesting a complete $\Delta\Delta^{14}\text{C}$ profile containing two minima, similar to profiles characterizing parts of the modern Atlantic [Key, 2004]. Regardless of the source of the higher $\Delta^{14}\text{C}$ at 1270 mwd, its presence clearly requires that the low- $\Delta^{14}\text{C}$ anomaly at 705 mwd arrived laterally since it could not have been produced by upward mixing of relatively high $\Delta^{14}\text{C}$ waters below.

We note that our reconstructed profiles and related conclusions are relatively robust to uncertainties in age modeling or differential bioturbation and dissolution, due to generally high sedimentation rates of the studied cores, averaging of signals over several thousand years for each time interval, and the fact that any age biases shared amongst cores during particular intervals will have little effect on estimated gradients of $\Delta^{14}\text{C}$. A recent suggestion that the benthic $\Delta^{14}\text{C}$ anomalies in PC08 are artifacts caused by the GISP2-tuned age model of PC08 [Davies-Walczak *et al.*, 2014] is incompatible with the large B-P ages (which are independent of the age model) that we observe coincident with the benthic anomalies in PC08 [Lindsay *et al.*, 2015] and now GC38 (Figure 5). This was also illustrated by use of an alternative age model, based on PC08 planktic ^{14}C and an assumption of constant surface reservoir age, which had little influence on the inferred magnitude and timing of the PC08 benthic $\Delta^{14}\text{C}$ anomalies ([Lindsay *et al.*, 2015] and related supported information). Removing the sedimentation rate limits used in our age modeling would result in slightly different $\Delta^{14}\text{C}$ estimates for PC10 and GC38, guided by more perfect *G. ruber* agreement with PC08, but the time-averaged $\Delta^{14}\text{C}$ depth gradients would not change substantially.

3.6. Lateral Water Mass Mixing and $\delta^{18}\text{O}$

In the previous section we argue that the anomalously low- $\Delta^{14}\text{C}$ carbon detected near Baja California must have arrived laterally during HS1 and the YD, leaving NPIW and EqPIW as possible proximal sources. Today, NPIW is characterized regionally by $\Delta^{14}\text{C}$ values that are ~15‰ lower than intermediate water near Baja California (Figure 1), but this horizontal gradient was apparently reversed during HS1 and the YD, when $\Delta^{14}\text{C}$ offsets from the coeval atmosphere in SBB core ODP 893a [Hendy *et al.*, 2002; Magana *et al.*, 2010] and other locations sampling NPIW [Okazaki *et al.*, 2010] indicate that NPIW $\Delta\Delta^{14}\text{C}$ was higher than that in intermediate waters near Baja California (Figure 7). This would suggest that EqPIW, as the only remaining proximal source of waters influencing the Baja California margin, had lower $\Delta\Delta^{14}\text{C}$ than waters at the location of PC08 during HS1 and the YD.

Presently, the only published radiocarbon reconstruction for EqPIW, from Galapagos Rise core VM21-30 [Stott *et al.*, 2009], is characterized by very low $\Delta\Delta^{14}\text{C}$, as might be expected (Figure 7). However, it is suspected that

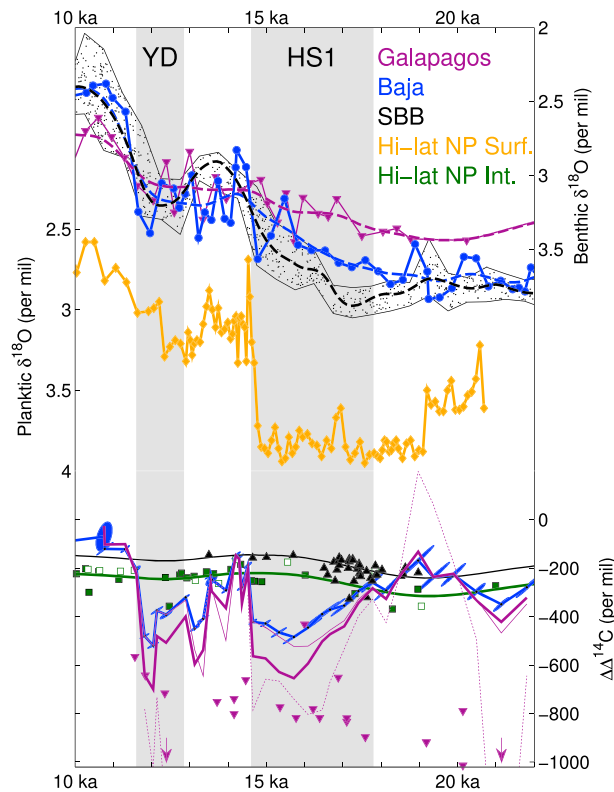


Figure 7. Comparison of regional $\delta^{18}\text{O}$ and $\Delta\Delta^{14}\text{C}$ records. (top) $\delta^{18}\text{O}$ data from Baja California core PC08 (blue filled circles and thin line, this study, bold dashed blue line is smoothing spline), Galapagos Rise core VM21-30 (purple inverted triangles and thin line) [Koutavas et al., 2006], shown on the age model of Stott et al. [2009] (bold dashed purple line is smoothing spline) and the 90th percentile range of 500 year windows of SBB cores ODP893A and MD2503 (black speckled envelope) [Hendy and Kennett, 2003; Hill et al., 2006] (bold dashed black line is smoothing spline). (middle) *N. pachyderma sinistral* $\delta^{18}\text{O}$ from core MD02-2489 (yellow diamonds) [Gebhardt et al., 2008] on the updated age model of Rae et al. [2014]. (bottom) Benthic $\Delta\Delta^{14}\text{C}$ from PC08 (blue solid line and 1σ error ellipses) [Lindsay et al., 2015; Marchitto et al., 2007], the Galapagos Rise (purple inverted triangles) [Stott et al., 2009], all available *Pyrgo*-free SBB data (black triangles) [Hendy et al., 2002; Magana et al., 2010], and a subset of the compilation of Okazaki et al. [2010] (north of 35°N and shallower than 1000 m from the NE Pacific, filled green squares) and NW Pacific (open green squares), with a smoothing spline to all data (solid green line). Also shown is estimated Galapagos Rise $\Delta\Delta^{14}\text{C}$ based on PC08 and estimated SBB $\Delta\Delta^{14}\text{C}$ (black line, equal to Okazaki spline fit plus 75‰), calculated using source water mixtures from modern *T* and *S* (bold purple line), unadjusted $\delta^{18}\text{O}$ gradients (thin dotted purple line), and adjusted $\delta^{18}\text{O}$ gradients (thin solid purple line). $\Delta\Delta^{14}\text{C}$ is calculated by subtracting coeval INTCAL13 $\Delta^{14}\text{C}$ from benthic $\Delta^{14}\text{C}$. PC08 $\Delta\Delta^{14}\text{C}$ error ellipses are 1 sigma and account for both marine and atmospheric uncertainties.

these results may be biased to anomalously low values by local sources of geologic ^{14}C -free carbon [Stott and Timmermann, 2011], leaving the ambient $\Delta\Delta^{14}\text{C}$ of EqPIW largely unconstrained. We therefore employ a simple mixing model in order to estimate the $\Delta\Delta^{14}\text{C}$ of EqPIW needed to explain the Baja California results. Because mixing ratios of EqPIW and NPIW off Baja California may have changed in the past, we consider three different scenarios. In the first we assume a fixed ratio of 2:1 (EqPIW:NPIW) at the location of PC08, as suggested by the modern hydrographic data, and apply a simple two end-member mixing models to project the expected $\Delta\Delta^{14}\text{C}$ of EqPIW in the vicinity of Galapagos Rise core VM21-30 (this estimate is referred to later as scenario 1). In the other two scenarios we make use of new and previously published benthic $\delta^{18}\text{O}$ results to estimate past water mass mixing ratios and projected $\Delta\Delta^{14}\text{C}$.

Based on changes in benthic $\delta^{18}\text{O}$ at SBB during deglaciation, Hendy and Kennett [2003] argued that less EqPIW reached the California margin during HS1, leading to higher benthic $\delta^{18}\text{O}$ at SBB, and that a sudden shift to lower benthic $\delta^{18}\text{O}$ at the start of BA represented a transition to a much greater supply of warm EqPIW (Figure 7). However, a more recent planktic *Neogloboquadrina pachyderma* $\delta^{18}\text{O}$ record from the Gulf of Alaska [Gebhardt et al., 2008; age model from Rae et al., 2014] also shows increasing values during HS1 followed by a rapid shift to lower values at the start of the BA (Figure 7), suggesting that deglacial $\delta^{18}\text{O}$ changes at SBB were largely a result of changes in North Pacific surface temperature and seawater $\delta^{18}\text{O}$ affecting the NPIW end-member rather than changes in EqPIW:NPIW mixing ratios as previously suggested by Hendy and Kennett [2003].

We present new $\delta^{18}\text{O}$ results obtained in *Uvigerina* spp. for core PC08 (for discussion of $\delta^{13}\text{C}$ data see supporting information and supporting information Figure S3) that when compared to the SBB $\delta^{18}\text{O}$ results and the *Uvigerina* spp. $\delta^{18}\text{O}$ results from Galapagos Rise core VM21-30 [Koutavas et al., 2006] (age model from Stott et al. [2009]) provide an additional constraint on north-south mixing along the California margin (Figure 7). In the modern ocean, these three sites lie close to the same density level (Figure 3), and we expect only very

small differences between the $\delta^{18}\text{O}$ of benthic calcite at SBB and Galapagos Rise (within $\sim 0.2\text{‰}$, supporting information Text S3) due to small and offsetting differences in modern annual average T and seawater $\delta^{18}\text{O}$ (cf. Figures 2 and 3 for T and S). In contrast to the modern situation, a significant $\delta^{18}\text{O}$ difference is seen during the LGM between similar benthic species in the Galapagos Rise and the SBB records, which grows larger during early HS1 and then collapses at the start of the BA, primarily due to changes in the SBB record. The shift to higher $\delta^{18}\text{O}$ values near the start of HS1 in SBB is not present in the PC08 record, suggesting that the proportion of EqPIW at the Baja California site may have increased during HS1 relative to the LGM mixture. This inference, which assumes that the Galapagos Rise and SBB records continued to represent end-member source waters mixing along a similar density level to Baja California, is consistent with Nd isotope evidence from PC08 sediments [Basak *et al.*, 2010].

Based on this revised interpretation, we make use of $\delta^{18}\text{O}$ results from SBB, Baja California, and Galapagos Rise cores to obtain water mass mixing ratios at the site of Baja core PC08, assuming that all sites lie on the same density level and that $\delta^{18}\text{O}$ of calcite is a conservative tracer (reflecting the combination of temperature and $\delta^{18}\text{O}$ of water, with the latter able to decouple calcite $\delta^{18}\text{O}$ from density). Specifically, mixing ratios were determined from the proportional difference between spline fits to the three $\delta^{18}\text{O}$ records at times when the $\delta^{18}\text{O}$ gradient between the Galapagos Rise and SBB splines was larger than 0.05‰ . Mixing ratios were then applied to coeval $\Delta\Delta^{14}\text{C}$ estimates from SBB core ODP 893a and Baja California core PC08 to yield an estimate of the $\Delta\Delta^{14}\text{C}$ at the site of core VM21-30 at Galapagos Rise (thin dotted purple line in Figure 7). Finally, we made a third estimate of mixing ratios and EqPIW $\Delta\Delta^{14}\text{C}$, correcting time-varying $\delta^{18}\text{O}$ gradients for small density differences between the core locations today (medium purple line in Figure 7, $\delta^{18}\text{O}$ adjustment details in supporting information Text S3). Implausible mixture values were rectified to the nearest end-member (i.e., if PC08 $\delta^{18}\text{O}$ did not lie between the coeval end-member $\delta^{18}\text{O}$ values, we used 100% of the nearest one).

Given a constant modern-like EqPIW:NPIW ratio near Baja California (scenario 1, bold purple line in Figure 7), our mixing model requires $\Delta\Delta^{14}\text{C}$ in EqPIW during HS1 to be $\sim 50\text{--}175\text{‰}$ below measured values in PC08 but $200\text{--}500\text{‰}$ higher than the reconstruction from VM21-30 [Stott *et al.*, 2009]. Scenarios 2 and 3 result in estimates that bracket the estimated $\Delta\Delta^{14}\text{C}$ of EqPIW from scenario 1, due to fractional mixtures during most of the deglaciation that tend to be less (scenario 2) or more (scenario 3) than the constant 2:1 (EqPIW:NPIW) mixing ratio assumed in scenario 1. Scenario 2 likely underestimates the fractional contribution of EqPIW during deglaciation and generates several points that are either impossibly low or implausibly high (points above 0‰ at $\sim 19\text{ ka}$), but even the extreme estimates from mixing scenario 2 frequently lie above values indicated by VM21-30 ^{14}C measurements.

Compared to our estimates, the low LGM $\Delta^{14}\text{C}$ values of Stott *et al.* [2009] seem especially unlikely, given the lack of a measured $\Delta\Delta^{14}\text{C}$ gradient between Baja California and SBB at that time. During the BA, the collapse of the regional $\delta^{18}\text{O}_{\text{calcite}}$ gradient leaves water mass mixing ratios unconstrained, allowing for the possibility that the source mixture at Baja California changed substantially to one dominated by NPIW, isolating the site from any low- $\Delta^{14}\text{C}$ signal in equatorial waters. Alternatively, if the Baja California source water mixture remained comparable to the modern one, deglacial EqPIW $\Delta^{14}\text{C}$ must have shifted rapidly from relatively low to relatively high values, as suggested by our estimate from scenario 1.

Overall, these estimates suggest that reasonable water mass mixing scenarios do not require anomalously low $\Delta^{14}\text{C}$ in EqPIW at the location of Galapagos Rise core VM21-30 and support the view that local geologic sources of ^{14}C -dead CO_2 [Stott and Timmermann, 2011] or age model bias may have influenced that record. If there was a local volcanic source that affected the VM21-30 record, it is unlikely to have played a significant role in controlling deglacial ocean and atmosphere CO_2 and $\Delta^{14}\text{C}$ more broadly, due to mass balance and alkalinity constraints. For example, the quantity of ^{14}C -dead carbon that would have to be added to seawater in order to reduce its $\Delta^{14}\text{C}$ signature by $\sim 200\text{‰}$ is $\sim 25\%$ of the preexisting dissolved inorganic carbon (DIC) pool. Adding that proportion of unbuffered DIC would increase the DIC:alkalinity ratio, causing carbonate ion concentrations to drop by approximately 90% and carbonate preservation to decline dramatically. However, carbonate preservation in Baja California core PC08 actually improved during deglacial ^{14}C depletion events relative to surrounding intervals [Ortiz *et al.*, 2004; Lindsay *et al.*, 2015], suggesting that any shallow plume of volcanic carbon was highly localized and did not reach the Baja margin. Indeed, preliminary results from at

least one new record from Galapagos Rise itself do not show the largest depletions evident in core VM21-30 [Bova and Herbert, 2014].

3.7. Evidence for a Deep Ocean Source of ^{14}C -Depleted DIC

There is growing evidence for widespread ^{14}C depletion in the deep Pacific and Southern Oceans during the LGM [Sikes *et al.*, 2000; Skinner *et al.*, 2010, 2014; Burke and Robinson, 2012; de la Fuente *et al.*, 2015; Keigwin and Lehman, 2015; Ronge *et al.*, 2016], and several cores in the 2.5–3.8 km depth range indicate $\Delta^{14}\text{C}$ as low or lower than our records from the Baja California margin during early HS1 [Skinner *et al.*, 2010; de la Fuente *et al.*, 2015; Ronge *et al.*, 2016]. Thus, there appear to be deep ocean sources of DIC having $\Delta^{14}\text{C}$ signatures low enough to explain our observations, and the presence of still more depleted sources cannot yet be ruled out. However, two substantial issues remain. First, no records yet document anomalously low $\Delta^{14}\text{C}$ in the deep ocean extending into the latter half of the deglaciation, as would seem to be required by our Baja California results during the YD and late BA. Second, the routing of low- $\Delta^{14}\text{C}$ waters from the deep ocean to parts of the upper ocean where deglacial $\Delta^{14}\text{C}$ minima have so far been documented remains unclear; as yet there is no direct evidence for anomalously low $\Delta^{14}\text{C}$ in present-day source areas and pathways of AAIW in the Southern Hemisphere [De Pol-Holz *et al.*, 2010; Rose *et al.*, 2010; Cléroux *et al.*, 2011; Sortor and Lund, 2011; Burke and Robinson, 2012; Siani *et al.*, 2013], which is otherwise expected based on evidence for renewed upwelling of ^{14}C -depleted Circumpolar Deep Water during deglaciation [Anderson *et al.*, 2009; Skinner *et al.*, 2010, 2014; Burke and Robinson, 2012].

Whether the existing deep ocean $\Delta^{14}\text{C}$ reconstructions can be explained entirely by ingrowth and aging of DIC due to reduced ventilation during glacial times [Broecker and Peng, 1986; Schmittner, 2003; Butzin *et al.*, 2005; Skinner *et al.*, 2014] or require an additional and possibly widespread source of ^{14}C -dead, geologic carbon emanating from deep ocean ridges in response to hydroisostatic changes [cf. Lund and Asimov, 2011] is not directly addressed by our analysis of the upper ocean records in this work.

4. Conclusions

Our results and analysis indicate that middepth depletion events observed off of the Baja California margin were proximally sourced from equatorial intermediate waters, and we speculate that these waters acquired their anomalous $\Delta^{14}\text{C}$ signature from distal sources in the deep Southern and/or Pacific Oceans [Sikes *et al.*, 2000; Skinner *et al.*, 2010, 2014; Burke and Robinson, 2012; de la Fuente *et al.*, 2015; Keigwin and Lehman, 2015; Ronge *et al.*, 2016]. Large B-P ages during HS1 and YD observed previously in PC08 [Lindsay *et al.*, 2015] and in new results from core GC38 presented here confirm that deglacial ^{14}C anomalies near Baja California reflect real changes in ocean chemistry and cannot be dismissed as artifacts of age model bias. The vertical structure of $\Delta^{14}\text{C}$ gradients revealed by our depth transect is similar to the modern gradient during the LGM and early BA but contains a pronounced middepth minimum during HS1, late BA, and the YD, ruling out local vertical mixing as the source of anomalously aged carbon during deglacial ^{14}C -depletion events. Inspection of the $\Delta^{14}\text{C}$ differences between intermediate-depth cores in the Eastern Equatorial and North Pacific further indicates that observed anomalies could not have been caused by southward penetration of NPIW and must have been due instead to compositional changes in deglacial EqPIW. Although shallow, localized volcanic sources of ^{14}C -dead CO_2 may have influenced some $\Delta^{14}\text{C}$ reconstructions in the region [Stott *et al.*, 2009; Stott and Timmermann, 2011], significant differences amongst individual reconstructions suggest that the influence was not widespread and could not have been large enough to influence the chemistry of the upper ocean and atmosphere as a whole. This continues to leave the deep ocean as the most likely source of aged, ^{14}C -depleted DIC influencing the upper ocean during deglaciation. The routing of these waters remains uncertain, but our analysis suggests that it must include the middepths of the Equatorial Pacific, pointing to an ultimate source in the deep Southern and Pacific Oceans.

References

- Allen, K. A., E. L. Sikes, B. Hönisch, A. C. Elmore, T. P. Guilderson, Y. Rosenthal, and R. F. Anderson (2015), Southwest Pacific deep water carbonate chemistry linked to high southern latitude climate and atmospheric CO_2 during the Last Glacial Termination, *Quat. Sci. Rev.*, 122, 180–191, doi:10.1016/j.quascirev.2015.05.007.
- Anderson, B. E., S. Ali, L. I. Bradtmiller, S. H. H. Nielsen, M. Q. Fleisher, and L. H. Burckle (2009), Wind-driven upwelling in the Southern Ocean and the deglacial rise in atmospheric CO_2 , *Science*, 323, 1443–1448.

Acknowledgments

We thank Lex van Geen for providing sediment samples; Chad Wolak, Patrick Cappa, Steve Morgan, and Derek Weller for laboratory assistance; and John Southon for AMS measurements. This work was funded by the NSF grant OCE-0851391 to S.J.L. and T.M.M. The new data presented in this paper are available in the supporting information. Comments from Elizabeth Sikes, Lex van Geen, and an anonymous reviewer helped us improve the manuscript.

- Bard, E. (1988), C ages measured in planktonic foraminifera: Paleocyanographic implications, *Paleocyanography*, 3(6), 635, doi:10.1029/PA003i006p00635.
- Basak, C., E. E. Martin, K. Horikawa, and T. M. Marchitto (2010), Southern Ocean source of ^{14}C -depleted carbon in the North Pacific Ocean during the last deglaciation, *Nat. Geosci.*, 3(11), 770–773, doi:10.1038/ngeo987.
- Bemis, B. E., H. J. Spero, and W. Lea (1998), Reevaluation of the oxygen isotopic composition of planktonic foraminifera: Experimental results and revised paleotemperature equations, *Paleocyanography*, 13(2), 150–160.
- Bostock, H. C., B. N. Opdyke, and M. J. M. Williams (2010), Characterising the intermediate depth waters of the Pacific Ocean using $\delta^{13}\text{C}$ and other geochemical tracers, *Deep Sea Res., Part I*, 57(7), 847–859, doi:10.1016/j.dsr.2010.04.005.
- Bova, S., and T. Herbert (2014), In pursuit of the mystery reservoir: Marine radiocarbon evidence from the eastern tropical Pacific for a deglacial CO_2 source, Abstract PP13D-05 presented at 2014 Fall Meeting.
- Broecker, W., and S. Barker (2007), A 190‰ drop in atmosphere's $\Delta^{14}\text{C}$ during the “Mystery Interval” (17.5 to 14.5 kyr), *Earth Planet. Sci. Lett.*, 256(1–2), 90–99, doi:10.1016/j.epsl.2007.01.015.
- Broecker, W. S., and T.-H. Peng (1986), Glacial to interglacial changes in the operation of the global carbon cycle, *Radiocarbon*, 28(2), 309–327.
- Bryan, S. P., T. M. Marchitto, and S. J. Lehman (2010), The release of ^{14}C -depleted carbon from the deep ocean during the last deglaciation: Evidence from the Arabian Sea, *Earth Planet. Sci. Lett.*, 298(1–2), 244–254, doi:10.1016/j.epsl.2010.08.025.
- Burke, A., and L. F. Robinson (2012), The Southern Ocean's role in carbon exchange during the last deglaciation, *Science*, 335(6068), 557–61, doi:10.1126/science.1208163.
- Burke, A., A. L. Stewart, J. F. Adkins, R. Ferrari, M. F. Jansen, and A. F. Thompson (2015), The glacial mid-depth radiocarbon bulge and its implications for the overturning circulation, *Paleocyanography*, 30, 1021–1039, doi:10.1002/2015PA002778.
- Butzin, M., M. Prange, and G. Lohmann (2005), Radiocarbon simulations for the glacial ocean: The effects of wind stress, Southern Ocean sea ice and Heinrich events, *Earth Planet. Sci. Lett.*, 235(1–2), 45–61, doi:10.1016/j.epsl.2005.03.003.
- Carriquiry, J. D., A. Sanchez, and G. Leduc (2015), Southern Ocean influence on the eastern tropical North Pacific's intermediate depth circulation during the Last Glacial Maximum, *Paleocyanography*, 30, 1132–1151, doi:10.1002/2014PA002766.
- Cl roux, C., P. deMenocal, and T. Guilderson (2011), Deglacial radiocarbon history of tropical Atlantic thermocline waters: Absence of CO_2 reservoir purging signal, *Quat. Sci. Rev.*, 30(15–16), 1875–1882, doi:10.1016/j.quascirev.2011.04.015.
- Cravatte, S., W. S. Kessler, and F. Marin (2012), Intermediate zonal jets in the tropical Pacific Ocean observed by Argo floats*, *J. Phys. Oceanogr.*, 42(9), 1475–1485, doi:10.1175/JPO-D-11-0206.1.
- Davies-Walczak, M., A. C. Mix, J. S. Stoner, J. R. Southon, M. Cheseby, and C. Xuan (2014), Late Glacial to Holocene radiocarbon constraints on North Pacific Intermediate Water ventilation and deglacial atmospheric CO_2 sources, *Earth Planet. Sci. Lett.*, 397, 57–66, doi:10.1016/j.epsl.2014.04.004.
- Dean, W. E., Y. Zheng, J. D. Ortiz, and A. van Geen (2006), Sediment Cd and Mo accumulation in the oxygen-minimum zone off western Baja California linked to global climate over the past 52 kyr, *Paleocyanography*, 21, PA4209, doi:10.1029/2005PA001239.
- de la Fuente, M., L. Skinner, E. Calvo, C. Pelejero, and I. Cacho (2015), Increased reservoir ages and poorly ventilated deep waters inferred in the glacial Eastern Equatorial Pacific, *Nat. Commun.*, 6, 7420, doi:10.1038/ncomms8420.
- Fiedler, P. C., and L. D. Talley (2006), Hydrography of the eastern tropical Pacific: A review, *Prog. Oceanogr.*, 69(2–4), 143–180, doi:10.1016/j.pcean.2006.03.008.
- Firing, E., S. E. Wijffels, and P. Hacker (1998), Equatorial subthermocline currents across the Pacific, *J. Geophys. Res.*, 103(C10), 21,413–21,423, doi:10.1029/98JC01944.
- Fleming, K., P. Johnston, D. Zwart, Y. Yokoyama, K. Lambeck, and J. Chappell (1998), Refining the eustatic sea-level curve since the Last Glacial Maximum using far- and intermediate-field sites, *Earth Planet. Sci. Lett.*, 163(1–4), 327–342, doi:10.1016/S0012-821X(98)00198-8.
- Galbraith, E. D., E. Y. Kwon, D. Bianchi, M. P. Hain, and J. L. Sarmiento (2015), The impact of atmospheric $p\text{CO}_2$ on carbon isotope ratios of the atmosphere and ocean, *Global Biogeochem. Cycles*, 29, 1–18, doi:10.1002/2014GB004929.
- Gebhardt, H., M. Sarnthein, P. M. Grootes, T. Kiefer, H. Kuehn, F. Schmieder, and U. R hl (2008), Paleonutrient and productivity records from the subarctic North Pacific for Pleistocene glacial terminations I to V, *Paleocyanography*, 23, PA4212, doi:10.1029/2007PA001513.
- van Geen, A., R. G. Fairbanks, P. Dartnell, M. McGann, J. V. Gardner, and M. Kashgarian (1996), Ventilation change in the northeast Pacific during the last deglaciation, *Paleocyanography*, 11(5), 519–528, doi:10.1029/96PA01860.
- van Geen, A., Y. Zheng, J. M. Bernhard, K. G. Cannariato, J. Carriquiry, W. E. Dean, B. W. Eakins, J. D. Ortiz, and J. Pike (2003), On the preservation of laminated sediments along the western margin of North America, *Paleocyanography*, 18(4), 1098, doi:10.1029/2003PA000911.
- Godwin, H. (1962), Half-life of Radiocarbon, *Nature*, 195(4845), 984.
- Hendy, I. L., and J. P. Kennett (2003), Tropical forcing of North Pacific intermediate water distribution during Late Quaternary rapid climate change?, *Quat. Sci. Rev.*, 22(5–7), 673–689, doi:10.1016/S0277-3791(02)00186-5.
- Hendy, I. L., J. P. Kennett, E. B. Roark, and B. L. Ingram (2002), Apparent synchronicity of submillennial scale climate events between Greenland and Santa Barbara Basin, California from 30–10 ka, *Quat. Sci. Rev.*, 21, 1167–1184.
- Hickey, B. M. (1979), The California Current System—hypotheses and facts, *Prog. Oceanogr.*, 8 (October 1978), 191–279.
- Hill, T. M., J. P. Kennett, D. K. Pak, R. J. Behl, C. Robert, and L. Beaufort (2006), Pre-Bolling warming in Santa Barbara Basin, California: Surface and intermediate water records of early deglacial warmth, *Quat. Sci. Rev.*, 25, 2835–2845, doi:10.1016/j.quascirev.2006.03.012.
- Keigwin, L. D., and S. J. Lehman (2015), Radiocarbon evidence for a possible abyssal front near 3.1 km in the glacial equatorial Pacific Ocean, *Earth Planet. Sci. Lett.*, 425, 93–104, doi:10.1016/j.epsl.2015.05.025.
- Key, R. M. (2004), A global ocean carbon climatology: Results from Global Data Analysis Project (GLODAP), *Global Biogeochem. Cycles*, 18, GB4031, doi:10.1029/2004GB002247.
- Kohfeld, K. E., and Z. Chase (2011), Controls on deglacial changes in biogenic fluxes in the North Pacific Ocean, *Quat. Sci. Rev.*, 30(23–24), 3350–3363, doi:10.1016/j.quascirev.2011.08.007.
- Koutavas, A., P. B. deMenocal, G. C. Olive, and J. Lynch-Stieglitz (2006), Mid-Holocene El Ni o—Southern Oscillation (ENSO) attenuation revealed by individual foraminifera in eastern tropical Pacific sediments, *Geology*, 34(12), 993, doi:10.1130/G22810A.1.
- LeGrande, A. N., and G. A. Schmidt (2006), Global gridded data set of the oxygen isotopic composition in seawater, *Geophys. Res. Lett.*, 33, L12604, doi:10.1029/2006GL026011.
- Lindsay, C. M., S. J. Lehman, T. M. Marchitto, and J. D. Ortiz (2015), The surface expression of radiocarbon anomalies near Baja California during deglaciation, *Earth Planet. Sci. Lett.*, 422, 67–74, doi:10.1016/j.epsl.2015.04.012.
- Locarnini, R. A., et al. (2013), World Ocean Atlas 2013 Volume 1: Temperature, in *NOAA Atlas NESDIS 74*, vol. 1, edited by S. Levitus and A. Mishonov, National Oceanographic Data Center, Silver Spring, Md.
- Lund, D. C., and P. D. Asimow (2011), Does sea level influence mid-ocean ridge magmatism on Milankovitch timescales?, *Geochem. Geophys. Geosyst.*, 12, 1525–2027, doi:10.1029/2011GC003693.

- Lynn, R. J., and J. J. Simpson (1987), The California Current system: The seasonal variability of its physical characteristics, *J. Geophys. Res.*, *92*(7), 12,947–12,966, doi:10.1029/JC092iC12p12947.
- MacDougall, T. J., and P. M. Barker (2011), Getting started with TEOS-10 and the Gibbs Seawater (GSW) Oceanographic Toolbox, WG127 ed., SCOR/IAPSO.
- Magana, A. L., J. R. Southon, J. P. Kennett, E. B. Roark, M. Sarnthein, and L. D. Stott (2010), Resolving the cause of large differences between deglacial benthic foraminifera radiocarbon measurements in Santa Barbara Basin, *Paleoceanography*, *115*, PA4102, doi:10.1029/2010PA002011.
- Marchitto, T. M., S. J. Lehman, J. D. Ortiz, J. Flückiger, and A. van Geen (2007), Marine radiocarbon evidence for the mechanism of deglacial atmospheric CO₂ rise, *Science*, *316*(5830), 1456–9, doi:10.1126/science.1138679.
- Marcott, S. A., et al. (2014), Centennial-scale changes in the global carbon cycle during the last deglaciation, *Nature*, *514*(7524), 616–619, doi:10.1038/nature13799.
- Martínez-Botí, M. A., G. Marino, G. L. Foster, P. Ziveri, M. J. Henehan, J. W. B. Rae, P. G. Mortyn, and D. Vance (2015), Boron isotope evidence for oceanic carbon dioxide leakage during the last deglaciation, *Nature*, *518*, 219–222, doi:10.1038/nature14155.
- Mix, A. C., N. G. Pisias, R. Zahn, W. Rugh, C. Lopez, and K. Nelson (1991), Carbon 13 in Pacific Deep and Intermediate Waters, 0–370 ka: Implications for Ocean Circulation and Pleistocene CO₂, *Paleoceanography*, *6*(2), 205–226, doi:10.1029/90PA02303.
- Monnin, E., A. Indermühle, A. Dällenbach, J. Flückiger, B. Stauffer, T. F. Stocker, D. Raynaud, and J. M. Barnola (2001), Atmospheric CO₂ concentrations over the last glacial termination, *Science*, *291*(5501), 112–4, doi:10.1126/science.291.5501.112.
- Okazaki, Y., A. Timmermann, L. Menviel, N. Harada, A. Abe-Ouchi, M. O. Chikamoto, A. Mouchet, and H. Asahi (2010), Deepwater formation in the North Pacific during the Last Glacial Termination, *Science*, *329*(5988), 200–4, doi:10.1126/science.1190612.
- Ortiz, J. D. (2011), Application of visible/near infrared derivative spectroscopy to Arctic paleoceanography, *IOP Conf. Ser. Earth Environ. Sci.*, *14*, 012011, doi:10.1088/1755-1315/14/1/012011.
- Ortiz, J. D., S. B. O'Connell, J. DeViscio, W. Dean, J. D. Carriquiry, T. Marchitto, Y. Zheng, and A. van Geen (2004), Enhanced marine productivity off western North America during warm climate intervals of the past 52 ky, *Geology*, *32*(6), 521, doi:10.1130/G20234.1.
- De Pol-Holz, R., L. Keigwin, J. Southon, D. Hebbeln, and M. Mohtadi (2010), No signature of abyssal carbon in intermediate waters off Chile during deglaciation, *Nat. Geosci.*, *3*(3), 192–195, doi:10.1038/ngeo745.
- Rae, J. W. B., M. Sarnthein, G. L. Foster, A. Ridgwell, P. M. Grootes, and T. Elliott (2014), Deep water formation in the North Pacific and deglacial CO₂ rise, *Paleoceanography*, *29*, 1–23, doi:10.1002/2013PA002570.Received.
- Reimer, P. J., E. Bard, A. Bayliss, J. W. Beck, P. G. Blackwell, C. Bronk, R. Caitlin, E. B. Hai, and R. L. Edwards (2013), INTCAL13 and MARINE13 radiocarbon age calibration curves 0–50,000 years cal BP, *Radiocarbon*, *55*(4).
- Ronge, T. A., R. Tiedemann, F. Lamy, B. V. Alloway, R. De Pol Holz, K. Pahnke, J. Southon, and L. Wacker (2016), Radiocarbon constraints on the extent and evolution of the South Pacific glacial carbon pool, *Nat. Commun.*, *7*, 1–12, doi:10.1038/ncomms11487.
- Rose, K. A., E. L. Sikes, T. P. Guilderson, P. Shane, T. M. Hill, R. Zahn, and H. J. Spero (2010), Upper-ocean-to-atmosphere radiocarbon offsets imply fast deglacial carbon dioxide release, *Nature*, *466*(7310), 1093–7, doi:10.1038/nature09288.
- Schmittner, A. (2003), Southern Ocean sea ice and radiocarbon ages of glacial bottom waters, *Earth Planet. Sci. Lett.*, *213*, 53–62, doi:10.1016/S0012-821X(03)00291-7.
- Shakun, J. D., P. U. Clark, F. He, S. A. Marcott, A. C. Mix, Z. Liu, B. Otto-Bliesner, A. Schmittner, and E. Bard (2012), Global warming preceded by increasing carbon dioxide concentrations during the last deglaciation, *Nature*, *484*(7392), 49–54, doi:10.1038/nature10915.
- Siani, G., E. Michel, R. De Pol-Holz, T. Devries, F. Lamy, M. Carel, G. Isguder, F. Dewilde, and A. Laurantou (2013), Carbon isotope records reveal precise timing of enhanced Southern Ocean upwelling during the last deglaciation, *Nat. Commun.*, *4*, 2758, doi:10.1038/ncomms3758.
- Sikes, E. L., C. R. Samson, T. P. Guilderson, and W. R. Howard (2000), Old radiocarbon ages in the southwest Pacific Ocean during the last glacial period and deglaciation, *Nature*, *405*, 555–559.
- Skinner, L., I. N. McCave, L. Carter, S. Fallon, A. Scrivner, and F. Primeau (2014), Reduced ventilation and enhanced magnitude of the deep Pacific carbon pool during the last glacial period, *Earth Planet. Sci. Lett.*, *411*, 1–21, doi:10.1016/j.epsl.2014.11.024.
- Skinner, L. C., S. Fallon, C. Waelbroeck, E. Michel, and S. Barker (2010), Ventilation of the deep Southern Ocean and deglacial CO₂ rise, *Science*, *328*(5982), 1147–51, doi:10.1126/science.1183627.
- Sortor, R. N., and D. C. Lund (2011), No evidence for a deglacial intermediate water Δ14C anomaly in the SW Atlantic, *Earth Planet. Sci. Lett.*, *310*(1–2), 65–72, doi:10.1016/j.epsl.2011.07.017.
- Spero, H. J., and D. W. Lea (2002), The cause of carbon isotope minimum events on glacial terminations, *Science*, *296*(5567), 522–5, doi:10.1126/science.1069401.
- Stott, L., and A. Timmermann (2011), Hypothesized link between glacial/interglacial atmospheric CO₂ cycles and storage/release of CO₂-rich fluids from deep-sea sediments, in *Abrupt Climate Change: Mechanisms, Patterns, and Impacts*, edited by H. Rashid, L. Polyak, and E. Mosley-Thompson, pp. 123–138, AGU, Washington, D. C.
- Stott, L., J. Southon, A. Timmermann, and A. Koutavas (2009), Radiocarbon age anomaly at intermediate water depth in the Pacific Ocean during the last deglaciation, *Paleoceanography*, *24*, PA2223, doi:10.1029/2008PA001690.
- Stuiver, M., and H. Polach (1977), Reporting of 14C data, *Radiocarbon*, *19*(3), 355–363.
- Stuiver, M., P. J. Reimer, and R. W. Reimer (2005), CALIB 5.0. [www Program and Documentation], [Available at <http://calib.qub.ac.uk/calib/manual/chapter1.html>]
- Talley, L. D. (1993), Distribution and formation of North Pacific Intermediate Water, *J. Phys. Oceanogr.*, *23*, 517–537.
- You, Y. (2003), The pathway and circulation of North Pacific Intermediate Water, *Geophys. Monogr. Ser.*, *30*, 2291, doi:10.1029/2003GL018561.
- Zweng, M. M., et al. (2013), World Ocean Atlas 2013 Volume 2: Salinity, in *NOAA Atlas NESDIS 74*, vol. 2, edited by S. Levitus and A. Mishonov, pp. 39, National Oceanographic Data Center, Silver Spring, Md.